Statistical relation between maximum vertical velocity and surface precipitation of tropical convective clouds in a global nonhydrostatic aquaplanet experiment

Tomoe Nasuno[1, *] and Masaki Satoh[1,2]

[1] *Research Institute for Global Change, Japan Agency for Marine-Earth Science and Technology, Yokohama, Japan*

[2] *Center for Climate System Research, University of Tokyo, 5-1-5 Kashiwanoha, Kashiwa, Chiba, 277-8568, Japan*

Manuscript received 9 June 2009

Revised 9 May 2010

Revised 12 August 2010

Revised 31 August 2010

Revised 9 September 2010

Revised 30 September 2010

*Corresponding author: Dr. Tomoe Nasuno, Research Institute for Global Change, Japan Agency for Marine-Earth Science and Technology, 3173-25 Showa-machi, Kanazawa-ku, Yokohama, Kanagawa 236-0001, Japan. E-mail: nasuno@jamstec.go.jp

Abstract

This study investigated the properties of heavy precipitation and its associated vertical motion in an aquaplanet experiment with a 3.5-km mesh global cloud-system resolving model (GCRM). The statistics of precipitation and vertical velocity were examined in terms of the precipitation top height (PTH) and the maximum in-cloud vertical velocity in each column (w_max) for the grid points with the top 1% and 1–10% of the surface precipitation rate (pr_sfc) in the 10°N–10°S domain. To support the findings, realistic simulation cases were also analyzed.

In the columns with the top 1% (1–10%) of pr_sfc, peak frequencies of w_max height were found at z = 4–6 (1–4) km with the PTH several kilometers above that. Thermodynamic conditions were more humid and warmer in these columns than in the columns with average precipitation. These results were common to all simulation cases. Composite time evolution of convection with heavy surface precipitation was also examined for the aquaplanet experiment. The results suggest that the vigorous upward motion in the middle (lower) troposphere for columns with the top 1% (1–10%) of pr_sfc enabled efficient moisture transport from the boundary layer to the middle troposphere.

1. Introduction

The importance of tropical deep convection to global atmospheric circulation has been widely accepted since Riehl and Malkus (1958) first proposed the "hot tower hypothesis." Recently, however, controversy over the hot tower theory has reemerged, based on studies of long-term satellite observations (e.g., Liu et al. 2007) as well as cloud-resolving simulations (e.g., Fierro et al. 2009), which have indicated that occurrences of deep convective cores over tropical oceans were fewer than those originally assumed. The present study aims to gain insight into the properties of deep convection in a vast tropical domain using simulation data by a global cloud-system resolving model (GCRM).

A companion paper (Nasuno and Satoh 2010, hereafter referred to as NS10) describes the characteristics of tropical in-cloud vertical motion in a 3.5-km aquaplanet experiment using a GCRM (the Nonhydrostatic Icosahedral Atmospheric Model, NICAM). NS10 compares vertical profiles of simulated precipitation and latent heating with those observed by the Tropical Rainfall Measurement Mission (TRMM) and shows that the model reproduces the general morphology of precipitation and total latent heating profiles fairly well, although deficiencies of cloud representation are also noted (Masunaga et al. 2008; Satoh et al. 2010). NS10 majorly focuses on the time evolution of

convective updrafts and the relationship between thermodynamic conditions and vertical motions in the context of the multi-scale organization of convection. They argue that differences between active and suppressed regions of convection in the 3.5-km mesh aquaplanet experiment primarily reflect the large-scale structure of convective disturbances that were spontaneously generated in the model. Noticeably, strong vertical motion in the middle troposphere selectively occurs with heavy precipitation in NS10's analysis, although the frequency of such events is low. This finding is consistent with the results of recent studies reporting the rare occurrence of undiluted ascent in the tropics (Fierro et al. 2009; Liu et al. 2007; Zipser 2003).

The primary objective of this paper is to further investigate properties of the vertical motion and thermodynamic conditions, focusing on heavy precipitating events. For this purpose, the statistics of maximum vertical motion (w_max) in the columns with the top 1% and 1–10% of intense surface precipitation (pr_sfc) are analyzed in a similar manner to that described in NS10. To examine the robustness of the results, two realistic simulations using NICAM are also analyzed.

2. Simulation data and method of analysis

The aquaplanet experiments and realistic simulations were performed using NICAM (Satoh et al. 2008a). The experimental design of the aquaplanet case (hereafter referred to

as case A) has been described by Tomita et al. (2005). A zonally invariant sea surface temperature (SST) was assumed (Neale and Hoskins 2001), and ten days integration was performed with a horizontal mesh size of 3.5 km and 54 vertically stretched layers (z = 35 m to 40 km). Full-level snapshot data at the fifth day of integration and outputs at six levels (z = 35 m, 1 km, 2 km, 5 km, 10 km, and 14 km) at 10-min intervals for the following 3 h are analyzed in this study. Two other simulations (Miura et al. 2007a; Satoh et al. 2010) used a realistic land-ocean distribution with 40 vertically stretched layers (z = 80 m to 38 km). One is the global 3.5-km-mesh simulation, the design of which was described by Miura et al. (2007a). This case was initialized using the National Centers for Environmental Prediction (NCEP) final analysis data at 00UTC 25 December 2006 and integrated for 7 days (hereafter referred to as case R). The model dynamics and physics were approximately the same as those in the aquaplanet experiment, with the exception of revisions in the advection and turbulent schemes (Miura et al. 2007b). Data from seven snapshots at 1-day intervals are used in this study. The experimental design of the second simulation with a realistic land-ocean distribution was described by Satoh et al. (2010), where a horizontally stretched grid system (Tomita 2008a) was used (hereafter referred to as the case RS). This simulation was initialized at 00UTC 1 January 2007 using grid point values (GPV) from the Japan Meteorological Agency (JMA). Data from 24 snapshots at

1-h intervals in the domain of horizontal mesh sizes < 5 km (approximately within a 10-degree radius of a point located on the equator at 110°E) are analyzed here. A cloud microphysical scheme, including five prognostic variables for condensates (NSW6, Tomita 2008b), was used in the case RS, whereas a simple scheme including two prognostic variables for water condensates (Grabowski 1998, hereafter referred to as G98) had been used in the case A and R.

Precipitation top height (PTH) and maximum vertical velocity in precipitating air columns (w_max) are defined by the same criteria as used in NS10. The PTH is defined as the highest level of precipitating grids in the air columns, where precipitating grid points are identified by a precipitation rate > 0.3 mm h^{-1}. The precipitation rate is calculated from the vertical fluxes of precipitating condensates (i.e., rainwater and snow in the G98 scheme and rainwater, snow, and graupel in the NSW6 scheme). These are computed separately for each category of precipitating condensates and then summed. Here, the air-relative fluxes (mass of condensates × terminal velocities) are considered to facilitate interpretation of the results (NS10). The formulation of terminal velocities is similar to that of G98 (Eq. 17 and Fig. 2) and NSW6 (Eq. 28 of Tomita 2008b) [1],

[1] A density factor (square root of the ratio of air density at the ground level to that at each level) was multiplied for rainwater in NSW6.

assuming the Marshall-Palmer distribution for drop sizes of precipitating condensates. The terminal velocities of snow and rainwater by the G98 (NSW6) scheme in the simulations range from 0.6–1.4 (1.2–2.4) and 3–7 (2–4) m s^{-1}, respectively, while those for graupel (NSW6) range from 3–8 m s^{-1}. Surface precipitation rate (pr_sfc) is diagnosed from vertical flux of precipitating condensates at the lowest level. Magnitude and height of w_max are vertically surveyed for cloudy grid points in each air column (NS10 section 3.2). Statistics for the 10°N–10°S domain (on oceanic grid points for the realistic land-ocean distribution cases) are examined for all the simulation cases (cf. NS10; Satoh et al. 2008b; Takayabu 2002).

3. Results

Figure 1 shows the probability density function (PDF) of w_max in the case A. To investigate vertical motion associated with heavy precipitation, w_max is classified by the pr_sfc. The precipitation rate for the top 1% (10%) cumulative probability is 46 (7) mm h^{-1} (Fig. 1c). In the case R and RS, these rates are 50 (6.5) and 43 (5.8) mm h^{-1}, respectively (not shown). The PDF of w_max has approximately log-normal distributions for all categories, consistent with oceanic observations of convective updrafts (LeMone and Zipser 1980). The mean and standard deviations of w_max for the columns with the top 1% and 1–10% of pr_sfc and all the precipitating columns are (0.63, 0.23), (0.06,

1 0.28), and (−0.53, 0.44) in logarithm (Fig. 1a), leading to peak frequencies of w_max at
2 approximately 3, 1, and 0.3 m s^{-1}, respectively. The slopes of probability for the columns
3 with the top 1% of pr_sfc and for all the precipitating columns are nearly parallel in the
4 upper ranges of w_max (Fig. 1b), which indicate that these vigorous updrafts are
5 exclusively associated with the top few percentages of intense precipitation events.
6 Figure 2a presents average profiles of vertical velocity in the columns with the top 1%
7 and 1–10% of pr_sfc and all the precipitating columns for the three simulation cases.
8 Peak magnitudes of upward motion in the columns with the top 1% of pr_sfc are 5–7
9 times larger than those for the top 1–10%. The heights of the peak velocity are in the
10 middle troposphere (z = 4–6 km) for the top 1% and higher than those for the top 1–10%
11 (z = 2–3 km). Thermodynamic conditions in the columns with heavy precipitation are
12 more humid below z = 12 km and warmer in z = 2–14 km than those averaged over all the
13 precipitating columns (Fig. 2b, c), indicating stronger latent heat release in the deep
14 troposphere in these columns. Figure 2d shows the average profiles of zonal wind, which
15 was dominant in the equatorial regions in the three experiments. In the case A, the vertical
16 shear of zonal wind in the columns with heavy precipitation is weaker than that averaged
17 over all the precipitating columns (Fig. 2d). Significant easterly shear in the case RS is
18 associated with a Madden-Julian Oscillation event (Satoh et al. 2010). Generally, the case

A and R are very similar in comparison with the case RS.

Figure 3 shows two-dimensional histograms of the height of occurrence of w_max and PTH. Histograms for the precipitating columns with w_max > 1 m s^{-1} are also presented, as well as those categorized by the pr_sfc. The fractions of these columns to all precipitating columns are 9.4, 11.1, and 8.0% for the case A, R, and RS, respectively. The frequency distributions for all the precipitating columns are nearly on the diagonal line, indicating precipitation production by upward motion around the PTH (Fig. 3a–c). In the frequency distributions for precipitating columns with w_max > 1 m s^{-1} and the columns with heavy surface precipitation, in contrast, w_max height is generally lower than the PTH (Fig. 3d–l), indicating the occurrence of w_max in organized convection with precipitating condensates already formed above (e.g., Fig. 12 of NS10). The height ranges of peak occurrence differ between the columns with the top 1% and 1–10% of pr_sfc in all the simulation cases. For the top 1% (1–10%), maximum occurrences of w_max height are found at z = 4–6 (1–4) km with the PTH a few kilometers above that (Fig. 3g–l). The probability distributions for the columns with w_max > 1 m s^{-1} (Fig. 3d–f) include double peaks. The peaks in the lower troposphere nearly coincide with those of the top 1–10% of pr_sfc columns (Fig. 3j–l). Such correspondence is not found in the upper troposphere, suggesting that updrafts (w_max > 1 m s^{-1}) in the upper

troposphere are not necessarily associated with heavy surface precipitation.

Temporal variation of the vertical motion and thermodynamic conditions in the columns with heavy precipitation is investigated using the six-level 10-min interval outputs of the case A. Maximum pr_sfc during the 3-h period are calculated in each column, and columns with maximum pr_sfc > 46 mm h^{-1} (7 mm h^{-1} < pr_sfc < 46 mm h^{-1}) are defined here as the "top 1% (1–10%) pr_sfc columns." Composite analyses for the pr_sfc categories are presented in Fig. 4, where the base time is equivalent to the time of maximum pr_sfc for each column.

In the top 1% (1–10%) pr_sfc columns, updraft cores are found at z = 5 (2) km at the time of maximum pr_sfc (Fig. 4a, b). Clouds (total condensates ≥ 0.2 x 10^{-3} kg kg^{-1}) are generated in the lower troposphere 2 (1) h prior to the peak pr_sfc, grow into the upper troposphere producing heavy precipitation (Fig. 4e), and remain suspended for more than 3 h. In both columns, transport of moisture from the boundary layer to the middle troposphere is obvious (Fig. 4c, d). The moistening and diabatic warming reach higher levels in the top 1% pr_sfc columns than in the top 1–10% pr_sfc columns. The top 1% pr_sfc columns are in a relatively moist environment with upward motion throughout the troposphere even after termination of precipitation (downward motion is formed in a thin layer near the surface). In the top 1–10% pr_sfc columns, moistening in the lower

troposphere also remains after the weakening of pr_sfc in subsiding motions.

4. Summary and Discussion

In this study, the statistical properties of vertical motion and thermodynamic conditions in columns with heavy precipitation are investigated using a global 3.5-km mesh aquaplanet experiment dataset (case A). Maximum vertical motion (w_max) in the top 1% and 1–10 % of intense surface precipitation (pr_sfc) is examined in a manner similar to that described in NS10. The same analyses for realistic simulations using the global (Miura et al. 2007a; case R) and regionally stretched (Satoh et al. 2010; case RS) NICAM are also presented to support the findings. In the global (regionally stretched) simulations, the cloud microphysical scheme of G98 (NSW6) is used.

Two-dimensional histograms of w_max height and precipitation top height (PTH) show peak occurrences of w_max at z = 4–6 (1–4) km for the top 1% (1–10%) of pr_sfc with the PTH a few kilometers above that. Thermodynamic conditions are more humid and warmer in the columns with heavy precipitation than in the columns with average precipitation. These properties are common to all three simulation cases and consistent with the results of NS10, where intense w_max in the middle troposphere selectively occurred in an active part of large-scale, well-organized convective systems.

The composite time evolutions of convection in the columns with the top 1% and

1–10% of pr_sfc are investigated for the aquaplanet experiment. The results show the occurrence of vigorous upward motion in the lower to middle troposphere in these columns, which enables efficient transport of moisture from the boundary layer to the middle troposphere. This finding is consistent with the results of NS10, where the category with w_max height in the middle troposphere produced the heaviest precipitation via a tight linkage between vertical motion and moist processes. The deep convection associated with very heavy precipitation events (top 1%) occurred within a warm, moist environment throughout the troposphere for the duration of the event lifecycles. Moistening effects in the lower troposphere by convection including low-level updrafts (e.g., top 1–10% pr_sfc columns) are also suggested.

Besides the similarity among the three simulation cases in the major points described above, differences are also noted in the mean profiles of temperature, moisture, and vertical motion. The results suggest significant impact of different cloud microphysical schemes. For example, temperature minimum in the middle troposphere (z = 4–6 km) associated with the melting process is formed in the case RS using the NSW6 scheme; this process was not considered in the G98 scheme. In the case RS, frequencies of w_max height at z = 8–12 km with PTH in the upper troposphere are more pronounced than those in the case A and R. A large amount of graupel, as well as snow, were produced in the

case RS (Satoh et al. 2010), and the peak frequency in the upper troposphere are attributable to cloud microphysical processes associated with them.

It is also possible that differences between the case RS and other two cases have been partly due to the limited domain of analysis in the former. For example, vertical wind shear was more pronounced over the regional domain for the case RS than that over the 10°N–10°S domain for the case R, which may have induced difference in mesoscale convective organization. The dependence on horizontal resolution is also a critical issue with respect to the statistics of vertical motion presented here (Khairoutdinov et al. 2009; Weisman et al. 1997). This preliminary study will be followed by further investigations using global simulation with the NSW6 scheme and sufficiently fine mesh sizes.

Acknowledgments

The authors are indebted to Drs. Hirofumi Tomita and Hiroaki Miura for providing the NICAM simulation datasets. Thanks are also extended to Drs. Shin-ichi Iga, Akira T. Noda, Kazuyoshi Oouchi, Hiroshi Taniguchi, and Chihiro Kodama for their cooperation and discussion, and to Ms. Mikiko Ikeda and Mr. Yohei Yamada for providing technical support. The authors acknowledge two anonymous reviewers for their helpful comments, which substantially improve the earlier version of the manuscript. The simulations were performed on the Earth Simulator. This research was supported by the Core Research for

Evolutional Science and Technology program of the Japan Science and Technology Agency, and by the Innovative Program of Climate Change Projection for the 21st Century (KAKUSHIN) project "Global Cloud Resolving Model Simulations toward More Accurate and Sophisticated Climate Prediction of Cloud/precipitation Systems," funded by the Ministry of Education, Culture, Sports, Science and Technology (MEXT), Japan.

References

Fierro, A. O., J. M. Simpson, M. A. LeMone, J. M. Straka, and B. F. Smull, 2009: On how hot towers fuel the Hadley cell: An observational and modeling study of line-organized convection in the equatorial trough from TOGA COARE. *J. Atmos. Sci*., **66**, 2730–2746.

Grabowski, W. W., 1998: Toward cloud resolving model of large-scale tropical circulations: a simple cloud microphysics parameterization. *J. Atmos. Sci*., **55**, 3283–3298.

Khairoutdinov, M. F., S. K. Krueger, C.-H. Moeng, P. E. Bogenschutz, and D. A. Randall, 2009: Large-eddy simulation of Maritime deep tropical convection. *J. of Adv. Model. Earth Syst.*, **1**, Art. #15, 13 pp., doi: 10.3894/JAMES.2009.1.15.

LeMone, M. A. and E. J. Zipser, 1980: Cumulonimbus vertical velocity events in GATE.

Part I: Diameter, intensity and mass flux. *J. Atmos. Sci.*, **37**, 2444–2457.

Liu, C., E. J. Zipser, and S. W. Nesbitt, 2007: Global distribution of tropical deep convection: Different perspectives from TRMM infrared and radar data. *J. Climate*, **20**, 489–503.

Masunaga, H., M. Satoh, and H. Miura, 2008: A joint satellite and global cloud-resolving model analysis of a Madden-Julian Oscillation event: Model diagnosis. *J. Geophys. Res*., **113**, D17210, doi:10.1029/2008JD009986

Miura, H., M. Satoh, T. Nasuno, A. T. Noda, and K. Oouchi, 2007a: An Madden-Julian Oscillation event simulated using a global cloud-resolving model. *Science*, **318**, 1763–1765.

Miura, H., H. Tomita, M. Satoh, A. T. Noda, T. Nasuno, and S. Iga, 2007b: A short-duration global cloud-resolving simulation under a realistic land and sea distribution. *Geophys. Res. Lett*., **34**, L02804, doi:10.1029/2006GL027448.

Nasuno, T. and M. Satoh, 2010: Properties of precipitation and in-cloud vertical motion in a global nonhydrostatic aquaplanet experiment. *J. Meteor. Soc*. *Japan*, submitted.

Neale, R. B. and B. J. Hoskins, 2001: A standard test for AGCMs including their physical parameterizations. I: The proposal. *Atmos. Sci. Lett*., **1,** 101–107.

Riehl, H. and J. S. Malkus, 1958: On the heat balance in the equatorial trough zone,

Geophysica, **6**, 503–538.

Satoh, M., T. Matsuno, H. Tomita, H. Miura, T. Nasuno, and S. Iga, 2008a: Nonhydrostatic Icosahedral Atmospheric Model (NICAM) for global cloud-resolving simulations. *J. Comput. Phys.*, the special issue on Predicting Weather, Climate, and Extreme events, 227, 3486-3514, doi:10.1016/j.jcp.2007.02.006.

Satoh, M., T. Nasuno, H. Miura, H. Tomita, S. Iga, and Y. Takayabu, 2008b: Precipitation statistics comparison between global cloud resolving simulation with NICAM and TRMM PR data. High Resolution Numerical Modelling of the Atmosphere and Ocean, Wataru Ohfuchi and Kevin Hamilton Eds, 99-112, ISBN-13: 978-0387366715, 293pp.

Satoh, M., T. Inoue, and H. Miura, 2010: Evaluations of cloud properties of global and local cloud-system resolving models using CALIPSO/CloudSat simulators. *J. Geophys.Res.*,115, D00H14, DOI:10.1209/2009JD012247, 2010.

Takayabu, N. Y., 2002: Spectral representation of rain profiles and diurnal variations observed with TRMM PR over the equatorial area. *Geophys. Res. Lett*., 29, 1584, doi:10.1029/2001GL014113.

Tomita, H., 2008a: A stretched grid on a sphere by new grid transformation. *J. Meteor. Soc. Japan*, **86A**, 107-119.

Tomita, H., 2008b: New micorphysics with five and six categories with diagnostic generation of cloud ice. *J. Meteor. Soc. Japan*, **86A**, 121-142.

Tomita, H., H. Miura, S. Iga, T. Nasuno, and M. Satoh, 2005: A global cloud-resolving simulation: Preliminary results from an aqua planet experiment. *Geophys. Res. Lett.*, **32**, L08805, doi:10.1029/2005GL022459.

Weisman, M, L., W. C. Skamarock, and J. B. Klemp, 1997: The resolution dependence of explicitly modeled convective systems. *Mon. Wea. Rev.,* **125**, 527–548.

Zipser, E. J., 2003: Some views on "Hot Towers" after 50 years of tropical field programs and two years of TRMM data. *Meteor. Monogr.* **29**, 49–58.

Figure captions

FIG. 1.

Probability of maximum in-cloud vertical velocity for each precipitating column (w_max) in the 10°N−10°S domain (open circle) and for columns containing the top 1% (closed circle) and 1−10% (cross) of surface precipitation rates (pr_sfc) in the case A. The abscissa (ordinate) is logarithmic in (a) ([b]). Log-normal distributions are also plotted (dashed lines) in (a). (c) Cumulative frequency of pr_sfc. The bin widths for w_max in (a) and (b) and for pr_sfc in (c) are 0.1 in logarithmic scale, 0.5 m s^{-1}, and 3 mm h^{-1},

1 respectively.

2 FIG. 2.

3 Average profiles of (a) vertical velocity, (b) relative humidity for water saturation, (c)
4 temperature difference, (d) zonal velocity for the precipitating columns with the top 1%
5 of pr_sfc (thick solid lines), top 1–10% of pr_sfc (thick broken lines), and all the
6 precipitating columns (thin lines) in the 10°N–10°S domain. In (c), differences from the
7 averages over all the precipitating columns are drawn. The case A (black lines), R (red
8 lines), and RS (blue lines) are presented. Averages in the 10°N–10°S domain are plotted
9 in the case A and R. Oceanic regions are used for the case R and RS.

10 FIG. 3.

11 Two-dimensional histograms of PTH and height of w_max for (a)–(c) all the
12 precipitating columns in the 10°N–10°S domain, precipitating columns with (d)–(f)
13 w_max > 1 m s^{-1}, (g)–(i) top 1% of pr_sfc, and (j)–(l) top 1–10% of pr_sfc. The case A (a,
14 d, g, j), R (b, e, h, k), and RS (c, f, i, l) are presented. The bin widths for PTH and w_max
15 height are 1 km. The probabilities are vertically interpolated following the method of
16 NS10. Contour lines are drawn for 0.1% km^{-2} and 0.2% km^{-2} and at 0.5% km^{-2} intervals.
17 Broken lines indicate w_max height equals PTH.

18 FIG. 4

Time series of composite profiles of (a) (b) vertical velocity (color and red contour lines, m s^{-1}) and amount of total condensates (black contour lines, 1.0 x 10^{-3} kg kg^{-1}) and (c) (d) deviations of potential temperature (color, red contour lines, K) and water vapor content (black contour lines, 1.0 x 10^{-3} kg kg^{-1}) for the top 1% (a, c) and 1–10% (b, d) of pr_sfc in the case A. (e) Composite time series of pr_sfc for the precipitating columns with the top 1% (solid lines) and 1–10% (broken lines) of pr_sfc. In (c) and (d), deviations from the average over all the precipitating columns in the 10°N–10°S domain are presented. The base time of the composite is the time at which the maximum pr_sfc of the 3-h period occurred at each grid point. In (a) and (b), contour intervals for vertical velocity are at 1.0 m s^{-1} and 0.1 m s^{-1} (< 0.5 m s^{-1}), and those for total condensates are 1.0 x 10^{-3} kg kg^{-1} and 0.2 x 10^{-3} kg kg^{-1} (<1.0 x 10^{-3} kg kg^{-1}). In (c) and (d) contour lines for water vapor deviations are drawn at 0.2 x 10^{-3} kg kg^{-1} and 1.0 x 10^{-3} kg kg^{-1} intervals.

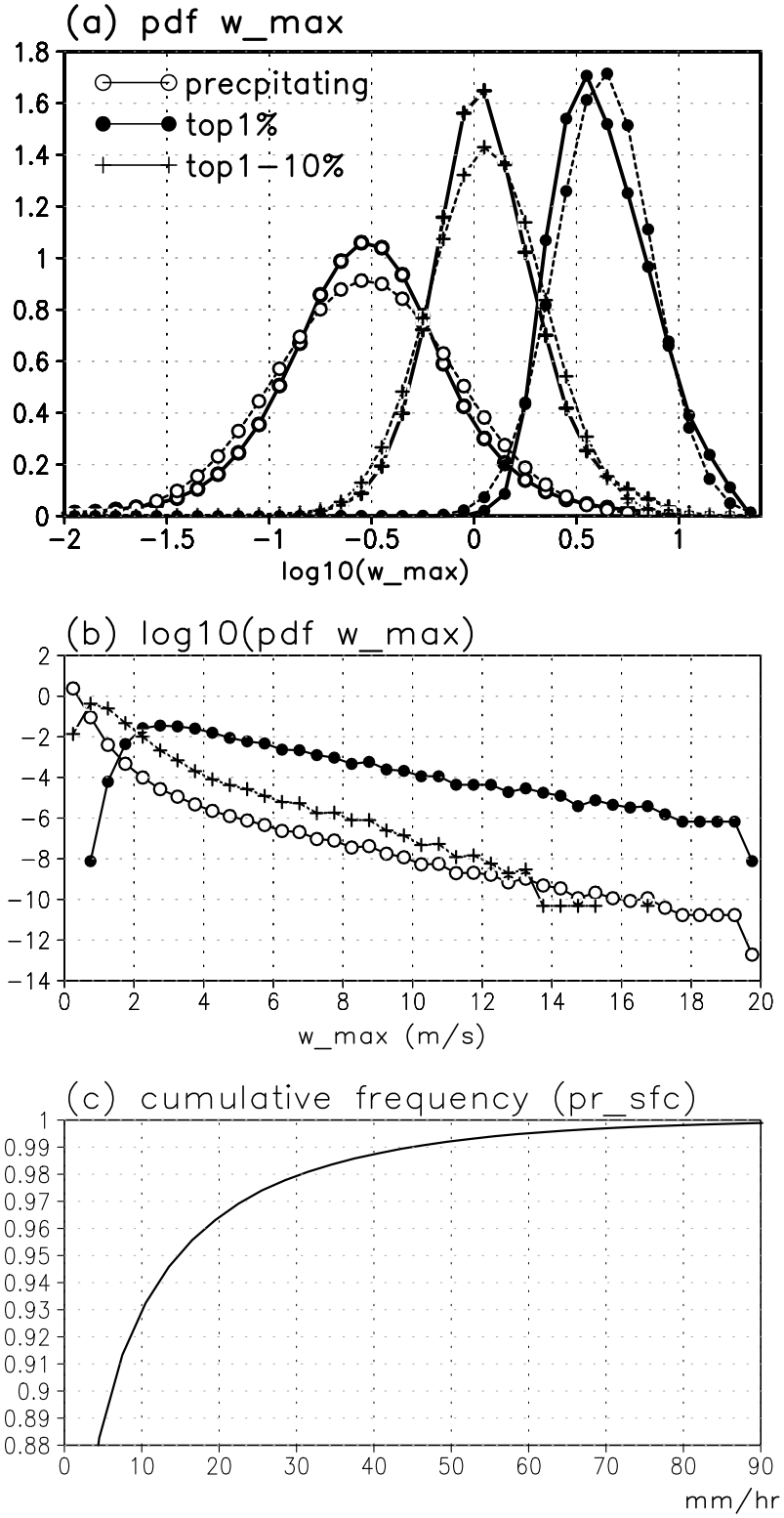

FIG.1 Probability of maximum in-cloud vertical velocity for each precipitating column (w_max) in the 10°N-10°S domain (open circle) and for columns containing the top 1% (closed circle) and 1-10% (cross) of surface precipitation rates (pr_sfc) in the case A. The abscissa (ordinate) is logarithmic in (a)([b]). Log-normal distriburions are also plotted (dashed lines) in (a). (c) Cumulative frequency of pr_sfc. The bin widths for w_max in (a) and (b) and for pr_sfc in (c) are 0.1 in logarithmic scale, 0.5 m s^{-1}, and 3 mm h^{-1}, respectively.

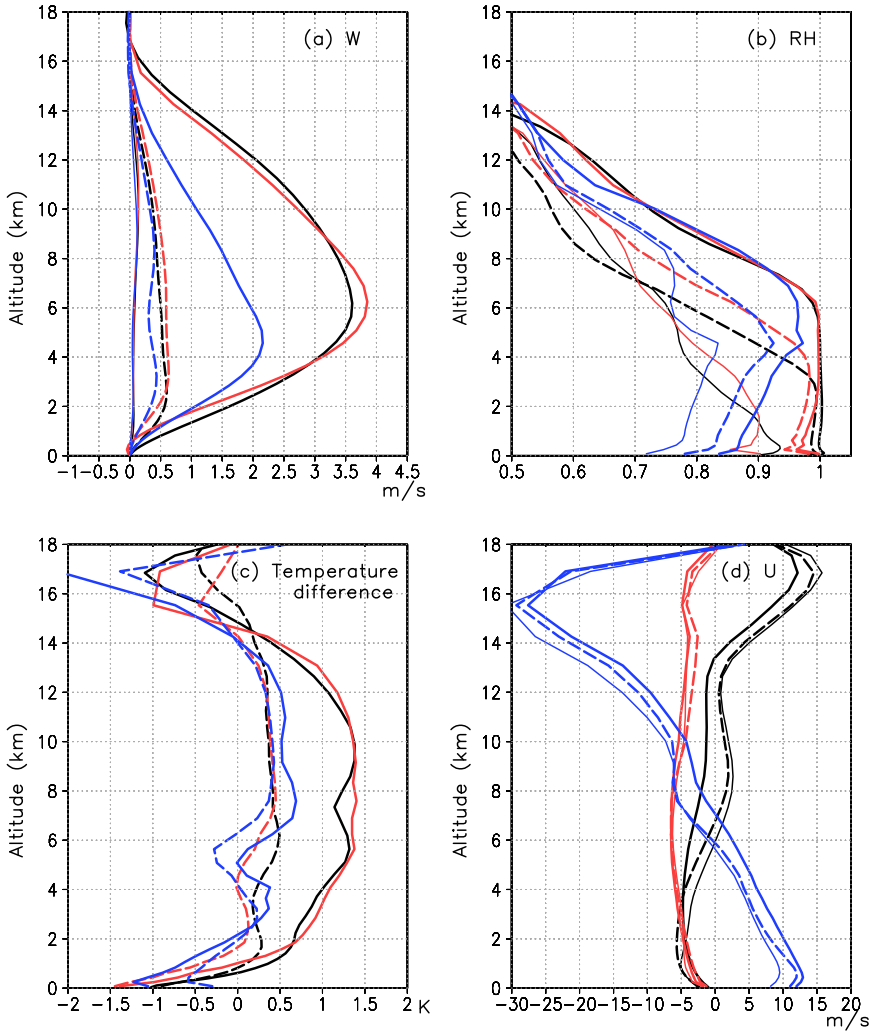

FIG.2 Average profiles of (a) verical velocity, (b) relative humidity for water saturation, (c) temperature difference,and (d) zonal velocity for the precipitating columns with the top 1% of pr_sfc(thick solid lines), top 1-10% of pr_sfc (thick broken lines), and all the precipitating columns(thin lines) in the 10°N-10°S domain. In (c), differences from the averages over all the precipitating columns are drawn. The case A (black lines), R (red lines), and RS (blue lines) are presented. Averages in the 10°N-10°S domain are plotted in the case A and R. Oceanic grid points are used for the case R and RS.

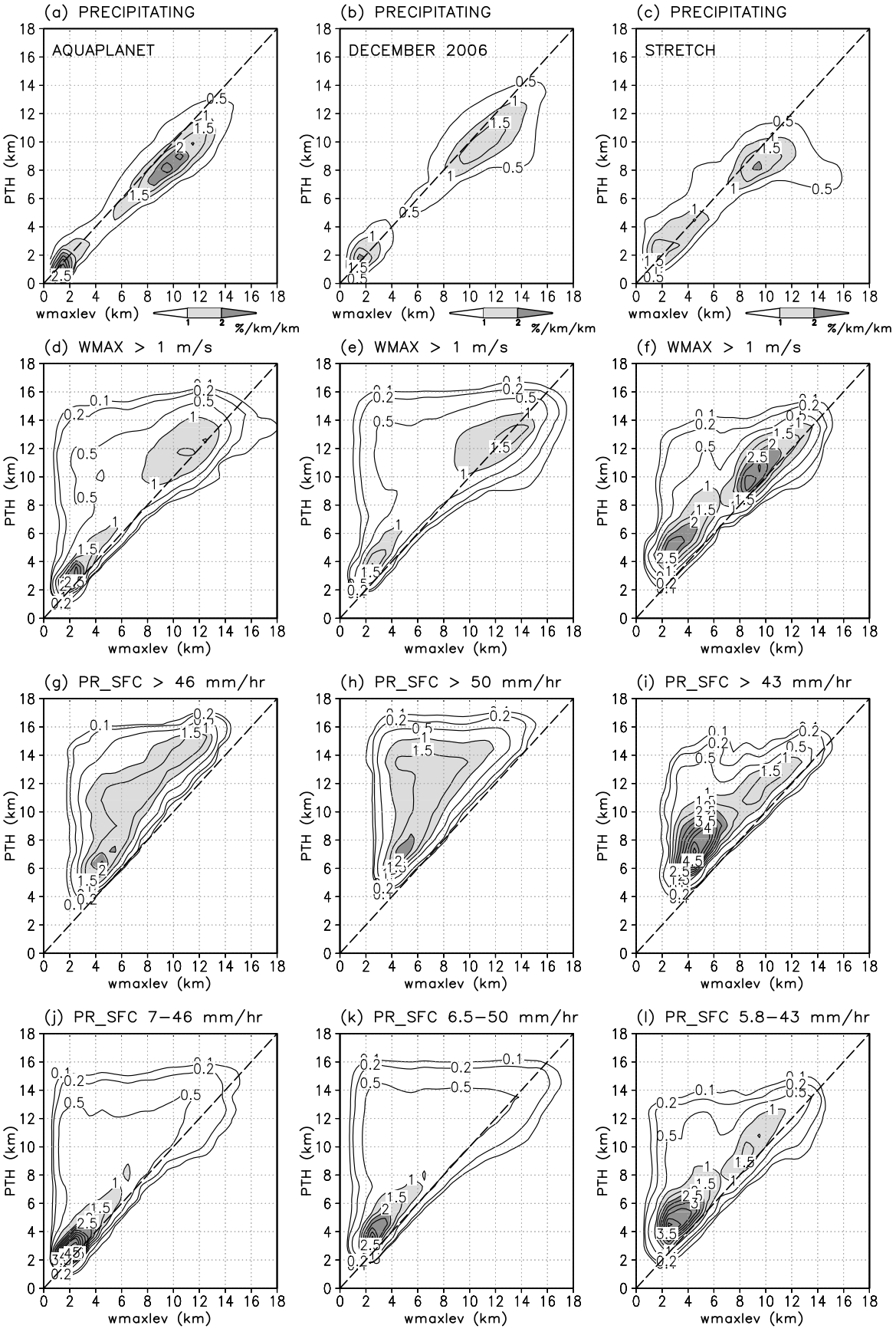

FIG.3 Two-dimensional histograms of PTH and height of w_max for (a)-(c) all the precipitating columns in the 10°N-10°S domain, precipitating columns with (d)-(f) w_max $>$ 1 m s $^{-1}$, (g)-(i) the top 1% of pr_sfc, and (j)-(l) the top 1-10% of pr_sfc. The case A (a, d, g, j), R (b, e, h, k), and RS (c, f, i, l) are presented. The bin widths for PTH and w_max height are 1 km. The probabilities are vetically interpolated following the method of NS10. Contour lines are drawn for 0.1% km^{-2} and 0.2% km^{-2} and at 0.5% km^{-2} intervals. Broken lines indicate w_max height equals PTH.

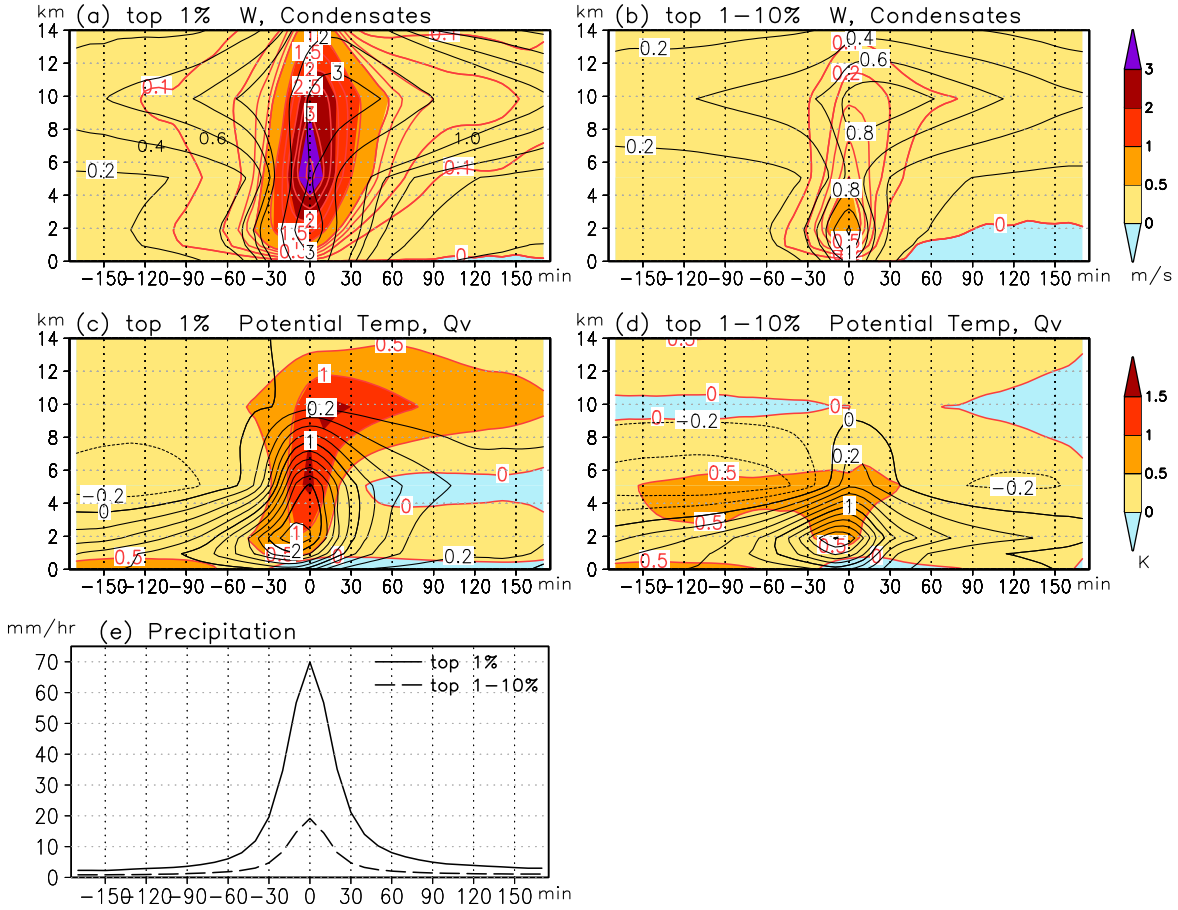

FIG.4 Time series of composite profiles of (a) (b) vertical velocity (color and red contour lines, m s^{-1}) and amount of total condensates (black contour lines, 1.0 x 10^{-3} kg kg^{-1}), and (c) (d) deviations of potential temperature (color, K) and water vapor content (black contour lines, 1.0 x 10^{-3} kg kg^{-1}) for the precipitating columns with the top 1% (a, c) and 1-10% (b, d) of pr_sfc in the case A. (e) Composite time series of pr_sfc for the precipitating columns with the top 1% (solid lines) and 1-10% (broken lines) of pr_sfc. In (c) and (d), deviations from the averages over all the precipitating columns in the 10°N-10°S domain are presented. The base time of the composite is the time at which the maximum pr_sfc for the 3-h period occurred at each grid point. In (a) and (b), contour intervals for vertical velocity are at 1.0 m s^{-1} and 0.1 m s^{-1} (< 0.5 m s^{-1}), and those for total condensates are 1.0 x 10^{-3} kg kg^{-1} and 0.2 x 10^{-3} kg kg (< 1.0 x 10^{-3} kg kg^{-1}). In (c) and (d), contour lines for water vapor deviations are drawn at 0.2 x 10^{-3} kg kg^{-1} and 1.0 x 10^{-3} kg kg^{-1} intervals.